International Journal of
MATERIALS RESEARCH

Zeitschrift für METALLKUNDE

Original Contributions

Iikka Isomäki[a], Marko Hämäläinen[a], Maria H. Braga[b], Michael Gasik[a]
[a] Department of Chemical and Metallurgical Engineering, School of Chemical Engineering, Aalto University, Espoo, Finland
[b] CEMUC, Physics Engineering Department, Engineering Faculty of the University of Porto, Porto, Portugal

First principles, thermal stability and thermodynamic assessment of the binary Ni–W system

The Ni–W binary system was assessed using critically evaluated experimental data with assistance from first principles analysis and the CALPHAD method. The solution phases (liquid, fcc-A1 and bcc-A2) were modeled using the substitutional regular solution model. The recently discovered Ni_8W metastable phase was evaluated as $Fe_{16}C_2$-like martensite with three sublattices, and shown to be possibly stable according to first principles calculations. Ni_8W was also modeled as an interstitial compound, but the model is not good because the solubility of tungsten in nickel is very low, especially at low temperatures. There is no experimental evidence for such low solubility. The other binary compounds Ni_4W and Ni_3W were assessed as stoichiometric ones. Compared independent experimental and first principles data agree well with the calculated phase diagram using updated thermodynamic parameters.

Keywords: Nickel; Tungsten; CALPHAD; First principles; Thermodynamic properties

1. Introduction

The nickel–tungsten system is a basis for many alloys and composites. For example, tungsten is a common solid solution strengthener in nickel-based superalloys, due to the creation of favorable strains in the crystal lattice and formation of suitable precipitates [1–3]. The Ni–W system is also an important part of the W–Ni–Fe–(Ti) system for heavy alloys, used for high density, structural and high-temperature applications (e. g. die casting dies, moulds, cores etc.) [4]. This subsystem with carbon is essential for different hard metals and cermets compositions [5]. The binary Ni–W coatings have been reported to be a reasonable alternative to hard chromium coatings due to their excellent tribological characteristics and mechanical properties [6–8], also having outstanding magnetic features [8, 9]. Ni-W compounds can have additional potential applications in catalysis, high-temperature electrodes and jewelry [7].

Due to the refractory nature of the systems with tungsten and related experimental challenges, first principles calculations are evidently an important tool to understand the thermodynamics and the variety of possible phases. Schindzielorz et al. [3] performed first principles calculations in the $0 \le x_W \le 0.33$ concentration range in the Ni–W system. These fcc-based structures were fully relaxed in two steps with the Vienna Ab Initio Simulation Package code (VASP) [10, 11] using the Perdew–Burke Ernzerhof (PBE) functional approximation as implemented in the standard generalized gradient approximation (GGA) [12] with projector augmented wave (PAW) pseudopotentials. A cluster-expansion (CE) method was used with the UNCLE code [13] and the heat of formation data were calculated. These energies were used for drawing the phase diagram at zero kelvin and Ni_4W and Ni_8W phases were found to be stable. These findings were confirmed by Kurz et al. [14, 15], who found Ni_8W (bct Pt_8Ti type) and Ni_4W (Ni_4Mo type) phases

to be stable, but Ni_3W phase (hcp-Cu_3Ti type) to be at least metastable.

In the analogous Ni–Mo system the metastable Ni_8Mo phase is known [7], so the Ni_8W might be also metastable. This would explain the difficulties related to experimental synthesis of the Ni_8W phase and contradictory findings reported in literature. Considering Ni_8W phase formation, known data of similar X_8Z-type intermetallics were analyzed here, where X is a Group VIII metal and Z is a group IV, V or VI transition metal. Sufficient experimental data were found for the following eleven X_8Z compounds (structural prototype Pt_8Ti): Pt_8V, Pt_8Zr, Ni_8Nb, Ni_8Ta, Ni_8V, Pd_8W, Pd_8V, Ni_8Mo, Pd_8Mo and Pt_8Cr [7]. It appears that Ni_8Z- and Pd_8Z-like phases all require excess vacancies for the ordering reaction to proceed at experimentally accessible conditions. Experimental evidence for some of these systems suggests that these X_8Z phases are thermodynamically stable [16], but this sadly was not experimentally studied in sufficient detail for Ni_8W. A complicated heat treatment with cold working or ion bombardment seems to be needed for formation of this phase for practically achievable and detectable amounts of the phase.

The tetragonal structure of the Ni_8W phase seems to be close to the $Fe_{16}C_2$ and $Fe_{16}N_2$ martensite [7, 17–19]. Badinier [20] studied both plate and lath-type martensites in the Fe–Ni–C system, and found that those regions might actually correspond to a carbide isomorph to well-known α''-$Fe_{16}N_2$ martensite found in Fe–N system. Brook [17, 18], Cardarelli [21] and Ishida et al. [22] have reported Fe–C and Fe–N martensites having tetragonal lattices of space group I4/mmm (D^{17}_{4h}; Pearson symbol tI18). In hard metals WC–(Fe–Ni–C) it was also found that the Fe–Ni–C binder phase shows fcc– to bct–martensitic transformation, raising the toughness of the bct-phase higher than in conventional WC–Co hard materials [23].

In this study both first principles calculations and thermodynamic assessment for the binary Ni–W system were carried out. The DFT (density functional theory) [24] calculations were made using VASP [10, 11, 25] and electronic energies per mole of atoms were determined at 0 K. Subsequently the PHONON direct method was used to determine Gibbs energies per mole of atoms at 298, 800 and 1 250 K [26]. Thermodynamic assessment was performed using the CALPHAD method.

2. Review of the experimental data

2.1. Phase diagram and activity data

Data for nine relevant phases considering the Ni–W binary system are discussed in this chapter.

Ellinger and Sykes [27], Kornilov and Budberg [28], Hofmann [29] and Gabriel et al. [30] give fcc Ni–W solid solubility values. All of these values are between 11 and 12.6 at.% tungsten in nickel in the temperature region of 500 to 1 073 K. Pearson's [31] phase boundary data are from 1 173 and 1 273 K, where no other data exist. Laugee et al. [32] and Udovskii et al. [33] solubility data agree well with each other. These values are all between 16.5 and 18.1 at.% W in the temperature range from 1 326 to 1 776 K. Meshkov et al. [34] used a galvanic cell for measuring tungsten activity for fcc nickel phase at 1 173 K. The fit between calculated and experimental data was quite good between 0 – 10 at.% tungsten.

Experimental data on Ni_8W are convenient to compare with its analogous Ni_8Mo phase. According to Mayer and Urban [35], in the Mo–Ni system bct-phase Ni_8Mo was found under 1 MeV electron irradiation from the Ni–Mo solid solution. Ordered Ni_8Mo phase develops from Ni–Mo solid solution at temperatures below 555 K. Sarma et al. [36] have studied samples, which were hot rolled at 1 373 K, then cold rolled, recrystallization annealed at 773 – 1 173 K and finally cold rolled again. X-ray diffraction (XRD) studies of these samples showed tungsten-rich precipitates in Ni-9 at.% W samples. They had a very large unit cell in comparison to Ni-based matrix and the composition was ∼12 at.% W, which is very near to 11.1 at.% W (Ni_8W). Maisel et al. [37] made X-ray diffuse scattering measurements on a Ni–W single crystal with 8 % W, and they showed {2/300} reflections, which suggest the presence of Pt_8Ti-type Ni_8 W.

Vogel [38] has made one of the first thermal and microscopic examinations of the Ni–W system, and he found a compound with approximate formula Ni_6W to exist up to 1 178 K. According to Becker and Ebert [39], Ni_6W might have face centered cubic structure. According to Taylor et al. [7], body centered tetragonal structure (bct) and face centered cubic (fcc) structures can be considered very close to each other. Later, however this Ni_6W phase has not been confirmed however.

Hofmann [29] found the Ni_4W phase with metallographic examination, XRD and differential thermoanalysis (DTA). Cury et al. [40] found Ni_4W compound in sintered and arc molten samples at 1 223 K with scanning electron microscopy + electron probe microanalysis (SEM + EPMA). Inomata and Kajihara [41] studied the Ni/W/Ni diffusion couples annealed 186 h at 1 173 K and 210 h at 1 023 K, where only the Ni_4W phase was found [41]. Okamoto [42] shows that well known phase Ni_4W is stable up to 1 275 K.

According to Mayer [35], Arapova et al. [43] and Okamoto [44] an analogous phase to Ni_3W, i.e. Ni_3Mo is a stable phase. Umanskii et al. [45] have found Ni_3W to be stable at 1 273 K after 100 h (cited by Hofmann [29]). Arapova et al. [43] have cold pressed Ni–W powder samples, then hardened them at 1 673 K and cooled in cooling furnace. Fcc-Ni and bcc-W phases were found with XRD after this procedure. However, in another work Arapova [46] has found with XRD that most intense hexagonal phase (Ni_3W) lines were superposed on the solid fcc-Ni and bcc-W. This makes detection of Ni_3W difficult.

After hardening and cooling with a cooling furnace, the samples were annealed in ampoules at 1 373 K 20 min, 1 h, 2 h, 5 h and 10 h. The type of quenching after annealing is unfortunately not mentioned. The result was that Ni_3W compound was found from samples annealed after deformation, therefore this compound could be metastable, at least at 1 373 K. During annealing at 1 373 K the amount of Ni_3W diminishes, which means metastability of the phase or that the temperature is over the dissociation temperature. The annealing temperature 1 373 K is over 850 K, where Ni_3W forms according to Kurz [14, 15]. The stability and metastability ratios of Ni_3W phase are related to different temperatures and conditions: Ni_3W is stable at lower temperatures and metastable at higher temperatures, which was reflected in the calculations made. Also Kurz

[14, 15] studied Ni–W thin film samples with XRD and transmission electron microscopy (TEM) and found that Ni_3W is (at least meta-)stable. The thin films were annealed 12 h at 850 K.

Walsh and Donachie [47] found NiW phase in diffusion couples, but the XRD study did not find intensities of peaks properly. However, the presence of NiW was detected with diffusion couples where surface contamination by carbon seems to occur.

Liu et al. [48] have analyzed diffusion bonded commercial purity Ni and Ni–W alloys at 1 473 K. In those diffusion couples Ni_6W_6C ($M_{12}C$) carbide was found. Cury et al. [40] showed that NiW phase found earlier is in fact Ni_6W_6C carbide phase. They could not find NiW in either arc melted or sintered samples. Lee et al. [49] have studied Ni–W thin films, annealed them at 1 573 K and they also found Ni_6W_6C compound. Marvel et al. [50] have also found Ni_6W_6C from electroplated and sputtered thin films with composition Ni-23 at.% W annealed at 973 K. This phase thus forms probably due to carbon contamination, which is difficult to avoid in practice.

Poulsen et al. [51] used W wires in pure Ni matrix and studied the samples with EPMA, and found NiW_2, but the intensity data is missing in that work.

Liu et al. [48] also have found carbide Ni_2W_4C in diffusion couples. This phase is similar to η-phase M_6C well-known in the Co–W–C system [40]. As for NiW, Cury et al. [40] showed that NiW_2 phase is in fact Ni_2W_4C phase. They could not find NiW_2 in arc melted samples. Lee et al. [49] found Ni_2W_4C compound from room temperature Kr-irradiated film, which was after that annealed at 1 123 K. As a conclusion, it was found that NiW is in fact the carbide Ni_6W_6C ($M_{12}C$) [40, 48–50] and NiW_2 is the carbide Ni_2W_4C (M_6C) [40, 48, 49], so these intermetallic compounds NiW and NiW_2 do not likely exist. Table 1 summarises the literature data for these Ni–W phases and used experimental methods

Therefore, the Ni–W system contains:

1. the liquid phase;
2. The terminal Ni solid solution (Ni) with quite large solid solubility for W;
3. The terminal W solid solution (W) with negligible solid solubility for Ni;
4. the stoichiometric compound Ni_8W; with decomposition temperature ∼800 K [3]
5. the stoichiometric compound Ni_4W with decomposition temperature 1 275 K [42] ; and
6. the stoichiometric compound Ni_3W with decomposition temperature ∼850 K [14].

Table 1. Ni–W phases, literature references and experimental data.

Phase	Reference	Experimental method
fcc-Ni	[27]	Metallography, X-ray diffraction (XRD)
	[28]	XRD, Metallography
	[29]	Metallography, XRD, differential thermoanalysis (DTA)
	[30]	DTA
	[31]	XRD
	[32]	Electromagnetic phase decantation, solid state annealing, XRD, DTA
	[33]	Calculation by free energy minimization algorithm
	[34]	Electromotive force (EMF) galvanic cell
Ni_8W	[36]	Hot rolling, cold tolling, recrystallization annealing, cold rolling, XRD
	[37]	X-ray diffuse scattering
"Ni_6W"?	[38]	Thermal and microscopic examination
	[39]	X-ray spectroscopy
Ni_4W	[27]	Metallography, XRD
	[29]	Metallography, XRD, DTA
	[40]	Electron probe microanalysis (EPMA), XRD
	[41]	Diffusion couples
	[42]	Review
Ni_3W	[14]	Thin films, Transmission electron microscopy (TEM)
	[15]	Thin films, TEM
	[43]	XRD
	[45]	XRD
	[48]	XRD
"NiW"	[28]	Diffusion couple, XRD
Ni_6W_6C ($M_{12}C$)	[40]	EPMA, XRD
	[48]	Diffusion couple, XRD, Scanning electron microscopy (SEM)
	[49]	Thin films, XRD, TEM
	[50]	Thin films, Scanning transmission electron microscopy (STEM), EPMA
"NiW_2"	[51]	EPMA
Ni_2W_4C (M_6C)	[40]	EPMA, XRD
	[48]	Diffusion couple, XRD, SEM
	[49]	Thin films, XRD, TEM

3. Calculations

3.1. First principles calculations

One of the most important methods of quantum mechanical modelling of solids is the framework of DFT [24] using the GGA [25]. In this work, DFT calculations with PAW pseudopotentials [52], and PBE functional [53] were used as implemented in the VASP code. A plane wave cutoff of at least 400.00 eV and k-spacings of $0.230 \times 0.230 \times 0.230$ Å^{-1} were used. Calculations were performed in the real space and for the following theoretically chosen nominal compositions: Ni, $Ni_{31}W$, $Ni_{15}W$, Ni_8W, Ni_4W, $Ni_{11}W_3$, $Ni_{15}W_4$, Ni_7W_2, Ni_3W, Ni_2W, Ni_7W_6, NiW, NiW_2 and W. The total energy was minimized with respect to the volume (volume relaxation), the shape of the unit cell (external relaxation), and the position of the atoms within the cell (internal relaxation). Magnetic moments were calculated using a spin polarized model.

The PHONON direct method [26] was engaged to predict the lattice dynamics using the harmonic approximation on VASP-minimized structures that had the lowest ground state energy. Therefore, the electronic structure at ground state was calculated using VASP and the zero point energy, the phonons' energy and the entropy were calculated using PHONON [26]. In fact, the Helmholtz free energy was obtained, which can be approximated to the Gibbs free energy at zero stress conditions.

The Helmholtz free energy, the internal energy (that can be approximated to the enthalpy) and the entropy were calculated after the vibration frequencies, ω, as follows Eqs. (1–3):

$$F_{\text{phonon}} = 3Nk_{\text{B}} \int_0^{\omega_{\text{L}}} \ln\left(\frac{2\sinh\hbar\omega}{2k_{\text{B}}T}\right) g(\omega)\mathrm{d}\omega \tag{1}$$

$$E_{\text{phonon}} = 3N \int_0^{\omega_{\text{L}}} \omega \coth\left(\frac{\hbar\omega}{2k_{\text{B}}T}\right) g(\omega)\mathrm{d}\omega \tag{2}$$

$$S_{\text{phonon}} = 3Nk_{\text{B}} \int_0^{\omega_{\text{L}}} \left[\frac{\hbar\omega}{2k_{\text{B}}T}\coth\left(\frac{\hbar\omega}{2k_{\text{B}}T}\right) - \ln\left(\frac{2\sinh\hbar\omega}{2k_{\text{B}}T}\right)\right] g(\omega)\mathrm{d}\omega \tag{3}$$

where N is the number of atoms in the cell, k_{B} is Boltzmann's constant, T the absolute temperature, ω_{L} the maximal frequency and $g(\omega)$ the frequency distribution function. Therefore by adding the electronic contribution (calculated using DFT as implemented in VASP) to the phonon contribution one could define $E(T)$ as the electronic plus vibrational energy of formation ($E_{\text{elec}} + ZPE + E_{\text{phonon}}(T)$), where ZPE is the zero-point energy $E(0\ K)$, $S(T)$ is the vibrational entropy at temperature T, and $F(T)$ is the electronic plus vibrational Helmholtz free energy, $F(T) = E(T) - T \cdot S(T)$.

3.2. Thermodynamic Assessment

Thermodynamic assessment in this work was based on previous thermodynamic evaluations of the ternary systems Ni–Ti–W by Dupin [54] and C–Ni–W by Gustafson et al. [55]. Thermodynamic parameters for liquid, bcc and fcc phases in the Ni–W system were taken from these previous studies. The Gibbs energy of the pure element, i, in a given structure, at a given absolute temperature, T, is represented by the following Eq. (4) [56]:

$${}^0G_i - H_i^{\text{SER}} = a + bT + cT\ln T + dT^2 + \frac{e}{T} + fT^2 + \ldots \tag{4}$$

where ${}^0G_i$ is absolute Gibbs free energy of the element, i, at T(K), and H_i^{SER} the enthalpy of the element in its reference state (Standard Element Reference, SER) at 298.15 K and 1 bar. The Gibbs energy functions for Ni and W above 298.15 K ($a \ldots f$ parameters) were taken from the SGTE (Scientific Group Thermodata Europe) compilation [56]. The Gibbs energies of the Ni_4W and Ni_3W compounds, at T (K), is written as follows Eq. (5):

$$G_c(T) = {}^0G_c - \sum_{i=1}^{2} x_i H_i^{\text{SER}} = A + BT + \sum_{i=1}^{2} x_i\left({}^0G_i - H_i^{\text{SER}}\right) \tag{5}$$

in which ${}^0G_c$ is the absolute Gibbs free energy of the compound, at T(K), and $\sum_{i=1}^{2} x_i H_i^{\text{SER}}$ the sum of the concentration-weighted enthalpy of each element in its reference state (A and B are the assessed parameters for compounds). Equation (6) was used for Gibbs energy for liquid phase:

$$G^{\text{Liq}}(T) = \sum_{i=1}^{2} x_i G_i^{0,\text{Liq}} + RT\sum_{i=1}^{2} x_i \ln x_i + G_{\text{m}}^{\text{E}} \tag{6}$$

here $\sum_{i=1}^{2} x_i G_i^{0,\text{Liq}}$ is the sum of each element's concentration versus its liquid phase Gibbs energy, $RT\sum_{i=1}^{2} x_i \ln x_i$ is the entropy-mixing term correspondent to the ideal mixture, in which R is the ideal gas constant. The Redlich–Kister equation [57] was used to represent the excess Gibbs energy of mixing G_{m}^{E} of the liquid phase Eq. (7):

$$G_{\text{m}}^{\text{E}} = x_{\text{Ni}}x_{\text{W}}\sum_{\nu=0}^{n} L_\nu (x_{\text{Ni}} - x_{\text{W}})^\nu, \text{ in which } L_\nu = a + bT \tag{7}$$

Thermo-Calc software version S and 2016a [58] was used to obtain the optimal parameter sets of A and B, and a and b.

The stability of the phases in the Ni–W system was assessed as follows. Liquid phase was assessed using one sublattice, fcc and bcc phases were assessed using two sublattices. According to Schindzielorz et al. [3], Taylor [7] and Kurz [14, 15] the phase Ni_8W is very probably a bct phase like Pt_8Ti. This structure is also considered as being similar to ordered tetragonal low temperature martensites α″-$Fe_{16}C_2$ and $Fe_{16}N_2$ [17–19].Therefore, the Ni_8W phase

was evaluated as $Fe_{16}C_2$ with three sublattices: for the Fe-C system they are usually $(Fe)_1(C,Va)_{1/8}(C,Va)_{23/8}$ [19]. Thermodynamic evaluation of $Fe_{16}C_2$ phase is based on bcc-Fe, but as the Ni structure is fcc-A1, magnetic terms for Ni_8W were taken from fcc-A1 (Ni) solid solution [8, 9], with six magnetic parameters. The sublattices used in Ni_8W were thus $(Ni)_1(W,Va)_{1/8}(W,Va)_{23/8}$. The Gibbs energy functions in the Ni : Va : W and Ni : W : Va sublattices have different coefficients compared with Fe : Va : C and Fe : C : Va.

Three sublattice model for martensite Ni_8W can be calculated with Eq. (8) [19], with the wildcard symbol (*) meaning any component could be present in the respective sublattice:

$$\begin{aligned} G_{\mathrm{m}}^{\mathrm{bct}} &= y_{Ni}^{(1)} y_{\mathrm{W}}^{(2)} y_{\mathrm{W}}^{(3)} G_{\mathrm{Ni:W:W}}^{\mathrm{bct}} + y_{Ni}^{(1)} y_{\mathrm{W}}^{(2)} y_{\mathrm{Va}}^{(3)} G_{\mathrm{Ni:W:Va}}^{\mathrm{bct}} \\ &+ y_{Ni}^{(1)} y_{\mathrm{Va}}^{(2)} y_{\mathrm{W}}^{(3)} G_{\mathrm{Ni:Va:W}}^{\mathrm{bct}} + y_{Ni}^{(1)} y_{\mathrm{Va}}^{(2)} y_{\mathrm{Va}}^{(3)} G_{\mathrm{Ni:Va:Va}}^{\mathrm{bct}} \\ &+ z_1 RT\left(y_{\mathrm{W}}^{(2)} \ln y_{\mathrm{W}}^{(2)} + y_{\mathrm{Va}}^{(2)} \ln y_{\mathrm{Va}}^{(2)}\right) \\ &+ z_2 RT\left(y_{\mathrm{W}}^{(3)} \ln y_{\mathrm{W}}^{(3)} + y_{\mathrm{Va}}^{(3)} \ln y_{\mathrm{Va}}^{(3)}\right) + {}^{\mathrm{E}}G_{\mathrm{m}}^{\mathrm{bct}} + {}^{\mathrm{mo}}G_{\mathrm{m}}^{\mathrm{bct}} \end{aligned} \tag{8}$$

with $z_1 = 1/8$ and $z_2 = 23/8$. The last term in Eq. (8) represents magnetic ordering and $y_i^{(S)}$ denotes the site fraction of component i on sublattice S. The term ${}^{\mathrm{E}}G_{\mathrm{m}}^{\mathrm{bct}}$ is the excess Gibbs energy described as in Eq. (9):

$${}^{\mathrm{E}}G_{\mathrm{m}}^{\mathrm{bct}} = y_{\mathrm{Ni}}^{(1)} y_{\mathrm{W}}^{(2)} y_{\mathrm{Va}}^{(2)} L_{\mathrm{Ni:W,Va:*}}^{\mathrm{bct}} + y_{\mathrm{Ni}}^{(1)} y_{\mathrm{W}}^{(3)} y_{\mathrm{Va}}^{(3)} L_{\mathrm{Ni:*:W,Va}}^{\mathrm{bct}} \tag{9}$$

and excess Gibbs energy consists as Eqs. (10–12):

$$L_{\mathrm{Ni:W,Va:*}}^{\mathrm{bct}} = \sum_{\nu} \left(y_{\mathrm{W}}^{(2)} - y_{\mathrm{Va}}^{(2)}\right)^{\nu} {}^{\nu}L_{\mathrm{Ni:W,Va:*}}^{\mathrm{bct}} \tag{10}$$

$$L_{\mathrm{Ni:*:W,Va}}^{\mathrm{bct}} = \sum_{\nu} \left(y_{\mathrm{W}}^{(3)} - y_{\mathrm{Va}}^{(3)}\right)^{\nu} {}^{\nu}L_{\mathrm{Ni:*:W,Va}}^{\mathrm{bct}} \tag{11}$$

$${}^{\mathrm{mo}}G_{\mathrm{m}}^{\mathrm{bct}} = RT \ln\left((\beta)^{\mathrm{bct}} + 1\right) f(\tau) \tag{12}$$

in Eq. (12) $(\beta)^{\mathrm{bct}}$ being the mean magnetic moment per mole of formula unit, $\tau = T/T_{\mathrm{C}}$ and T_{C} is Curie temperature. The alternative model for Ni_8W could be an interstitial solid solution like in fcc-TiC: $(Ti)_1(C,Va)_1$ [59]. In this study the model is $(Ni)_{0.889}(W,Va)_{0.111}$. Eq. (13) shows two sublattice interstitial model [60], $a = 0.889$ and $c = 0.111$ and Eq. (12) shows ${}^{\mathrm{mo}}G_{\mathrm{m}}^{\mathrm{Ni8W}}$.

$$\begin{aligned} G^{\mathrm{Ni_8W}}(T) &= y_{Ni} y_{\mathrm{W}} {}^{0}G_{\mathrm{Ni:W}} + y_{Ni} y_{\mathrm{Va}} {}^{0}G_{\mathrm{Ni:Va}} \\ &+ aRT(y_{\mathrm{Ni}} \ln y_{\mathrm{Ni}}) + cRT(y_{\mathrm{W}} \ln y_{\mathrm{W}} + y_{\mathrm{Va}} \ln y_{\mathrm{V}a}) \\ &+ y_{\mathrm{Ni}} y_{\mathrm{W}} L_{\mathrm{Ni:W}} + y_{\mathrm{Ni}} y_{\mathrm{Va}} L_{\mathrm{Ni:Va}} + y_{Ni} y_{\mathrm{W}} y_{\mathrm{Va}} L_{\mathrm{Ni:W,Va}} + {}^{\mathrm{mo}}G_{\mathrm{m}}^{\mathrm{Ni8W}} \end{aligned} \tag{13}$$

Tetragonal Ni_4W is a stable phase [29, 40–42] and it was thermodynamically evaluated as an intermetallic compound and considered to decompose at 1 275 K as in [42]. Hexagonal Ni_3W phase in Ni–W films was observed to be thermally stable at temperatures as high as 850 K, as evidenced by (XRD) before and after annealing treatments [14, 15] and was here also evaluated as a stoichiometric compound.

4. Results and discussion

The first principles calculations in this work show the stability of the phases at temperatures 0, 298, 800 and 1 250 K.

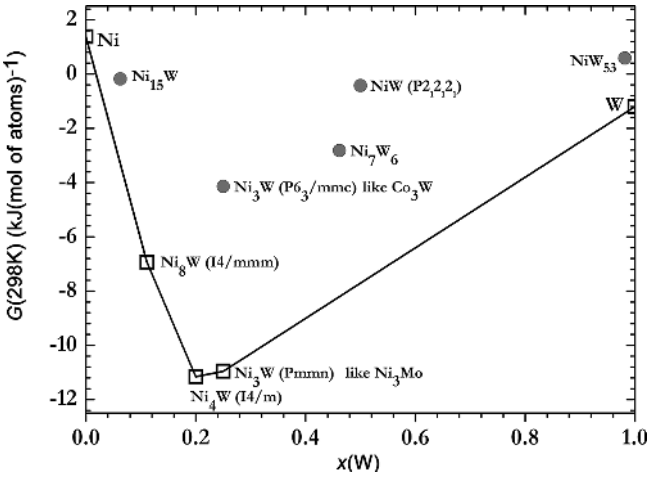

Fig. 2. Gibbs energies for the Ni–W system normalized for the number of moles of atoms at 298 K after DFT and phonon calculations. According to calculations Ni, Ni_8W, Ni_4W, Ni_3W and W were stable. Filled circles show unstable phases.

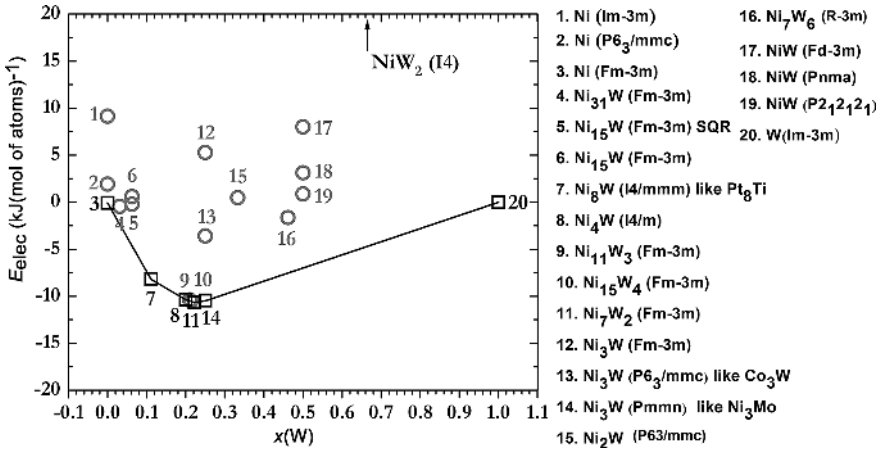

Fig. 1. Electronic energy of formation (VASP energy of formation) after this work. The ground state line is represented by the convex hull. According to this study the phases Ni (3), Ni_8W (7), Ni_4W (8), Ni_7W_2 (11), Ni_3W (14) and W (20) are stable at 0 K. Fifteen other phases marked with open circle were not stable.

Figure 1 shows electronic energies of formation for different phases at 0 K (stable phases are on the convex hull). Four compounds were found to be stable at 0 K: Ni_8W, Ni_4W, Ni_7W_2 and Ni_3W. For similar studies Schindzielorz et al. found Ni_7W_2 being stable [3], but Maisel et al. [37] and Kurz et al. [14, 15] did not. Because data on Ni_7W_2 are contradictory, Ni_7W_2 was omitted from thermodynamic assessment in this study.

With first principles calculations Schindzielorz et al. [3] agreed that Ni_8W and Ni_4W are stable compounds at 0 K.

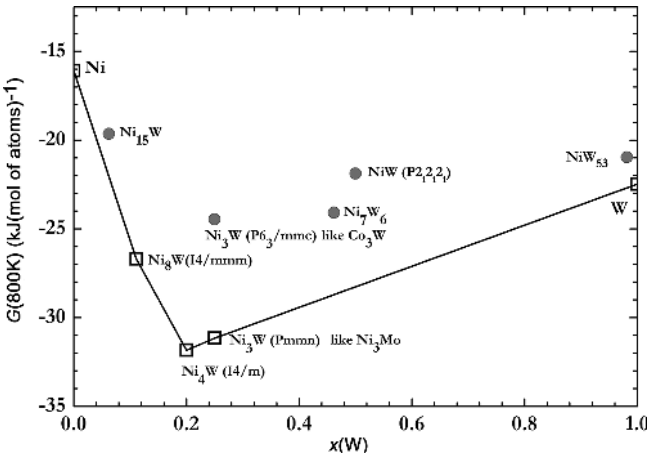

Fig. 3. Gibbs energies for the Ni–W system normalized as above at 800 K after DFT and phonon calculations. According to our calculations Ni, Ni_8W, Ni_4W, Ni_3W and W are stable. Filled circles show unstable phases.

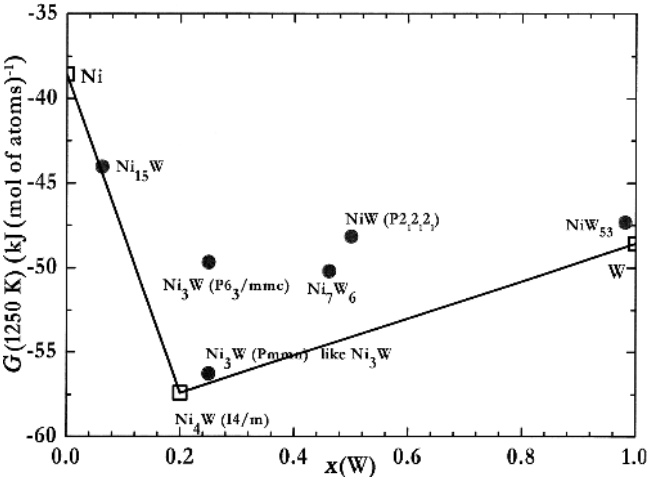

Fig. 4. Gibbs energies for the Ni–W system normalized as above at 1 250 K after DFT and phonon calculations. According to our calculations Ni, Ni_4W and W are stable. Filled circles show unstable phases.

Table 2. Compounds in the Ni–W system and their electronic energies comparable to the formation enthalpies at $T = 0$ K.

Compound	H_f (kJ (mol atoms)$^{-1}$) (this work)	H_f (kJ (mol atoms)$^{-1}$) [14]
Ni_8W	–8.50	–6.596
Ni_4W	–10.25	–10.231
Ni_3W	–10.38	–10.135
Ni_7W_2	–10.50	–10.617

Table 3. Compounds in the the Ni–W system and their formation Gibbs energies at 298 K.

Compound	G_f (kJ (mol atoms)$^{-1}$) (1st principles)	G_f (kJ (mol atoms)$^{-1}$) (CALPHAD) Martensitic Ni_8W References: Ni fcc-A1 and W bcc-A2	G_f (kJ (mol atoms)$^{-1}$) (CALPHAD) Interstitial Ni_8W References: Ni fcc-A1 and W bcc-A2
Ni_8W	–8.02	–11.25	–24.0
Ni_4W	–12.02	–11.31	–23.27
Ni_3W	–11.69	–11.34	–22.5

Table 4. Compounds in the Ni–W system and their structures.

Compound	Crystal structure	Prototype	Space Group	Space Group Number	Pearson Symbol	Strukturbericht
Ni_8W [7, 21, 63]	bct	Pt_8Ti Ni_8Mo $Fe_{16}N_2$ $Fe_{16}C_2$	I4/mmm	139	tI18	D2/g
Ni_8W [7, 59, 61, 63]	fcc	TiC	Fm3 m	225	cF8	B1
Ni_4W [14, 27, 63]	tetr	$MoNi_4$	I4/m	87	tI10	D1/a
Ni_3W [14, 63]	hcp	Cu_3Ti	Pmmn	62	OP8	D0/a
Ni_7W_2 [18, 61, 63]	fcc	NaCl	Fm3 m	225	cF8	B1

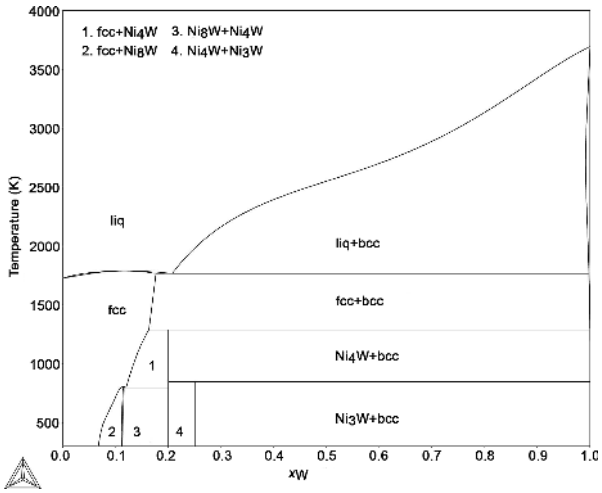

(a)

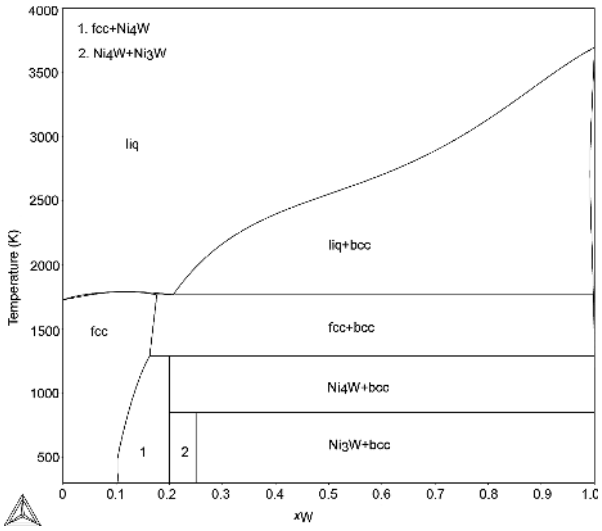

(b)

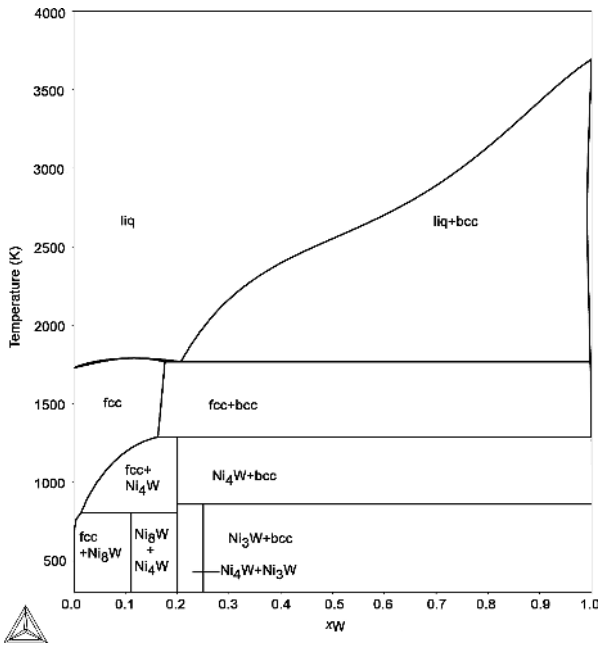

(c)

Fig. 5. (a) Ni–W phase diagram with Ni_8W. (b) Ni–W phase diagram without Ni_8W. (c) as (a), but with interstitially modeled Ni_8W.

Further, Kurz [14, 15] calculated, that Ni_3W is very close to stable phase (enthalpy of formation about –10.1 kJ mol^{-1} at 0 K), but only 144.7 J mol^{-1} above stability curve. Using our own data Fig. 2 shows the stable phases of Ni–W system at 298 K and Fig. 3 at 800 K, in both cases the stable compounds are Ni_8W, Ni_4W and Ni_3W. Figure 4 shows that at 1 250 K Ni_4W is the only stable compound. The Gibbs energy curve has the same shape in all cases. Table 2 shows

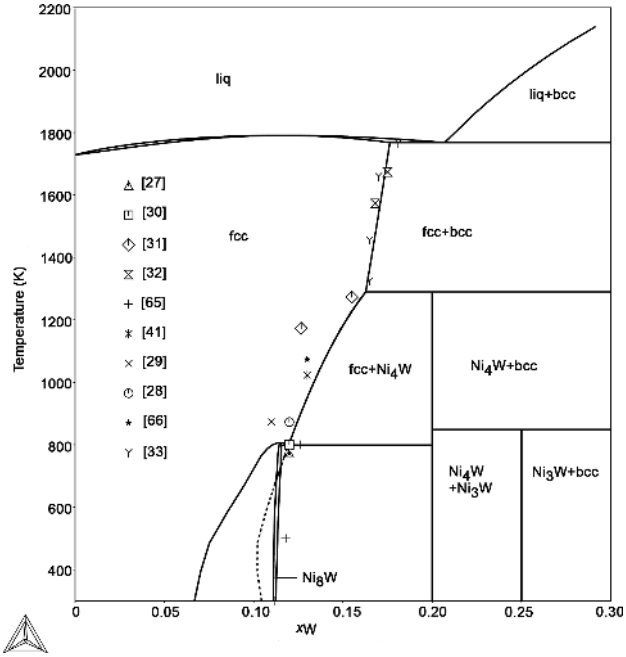

(a)

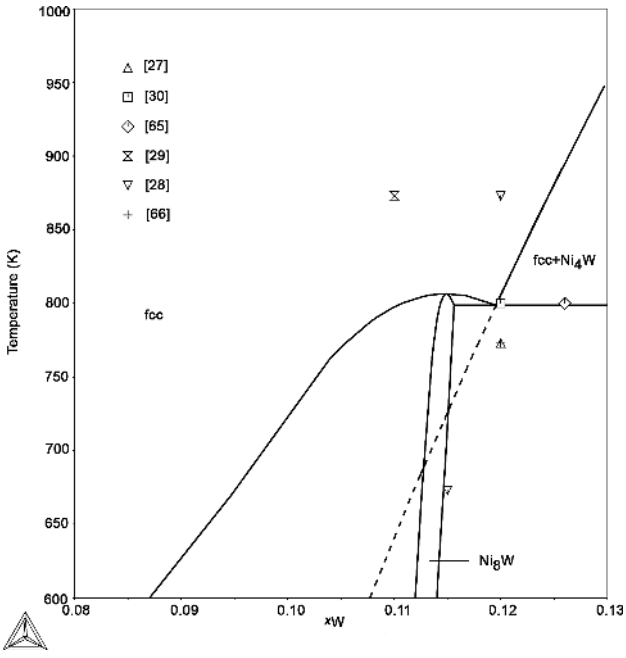

(b)

Fig. 6. (a) Ni–W phase diagram with and without Ni_8W (superimposed). Dashed curve shows the solid solution line. (b) Same figure, in which the surroundings of Ni_8W are zoomed. Dashed curve refers to the same as in (a). At temperatures above the dashed curve, the continuous curve is common for both cases, with or without Ni_8W. Figures were calculated with thermodynamic parameters evaluated by the authors. References for experimental data in [27–33, 42, 65, 66].

calculated enthalpies of formation (electronic energies) at $T = 0$ K from this work and in comparison with data by Kurz et al. [14]. Table 3 shows Gibbs energies of formation at 298 K for compounds in Ni–W system according to first principles calculations and calculated from both present thermodynamic assessment. The obtained Gibbs energy values according to first principles calculations and from present thermodynamic assessment are in a good agreement for

Table 5a. Thermodynamic parameters for the Ni–W system with martensitic Ni_8W.

Phase	Parameters (J(mol)$^{-1}$)	Source
Liquid phase, model (Ni,W)	${}^0L_{Ni,W} = -20\,470+7.55*T$ ${}^1L_{Ni,W} = -33\,545+15.2*T$ ${}^2L_{Ni,W} = -12\,400$	[54]
bcc_A2 phase, model $(Ni,W,Va)_1(Va)_3$	${}^0T^C_{Ni:Va} = 575$ ${}^0B^{magn}_{Ni:Va} = 0.85$ ${}^0L_{Ni,W} = +82\,000$	[55]
fcc_A1 phase, model (Ni,W)(Va)	${}^0T^C_{Ni:Va} = 633$ ${}^0B^{magn}_{Ni:Va} = 0.52$ ${}^0L_{Ni,W} = +2\,556+11.6*T$ ${}^1L_{Ni,W} = -52\,900$	[55]
Ni_8W phase, model $(Ni)(W,Va)_{0.125}(W,Va)_{2.875}$	${}^0T^C_{Ni:Va:Va} = +633$ ${}^0B^{magn}_{Ni:Va:Va} = +0.52$ ${}^0T^C_{Ni:Va:W} = +633$ ${}^0B^{magn}_{Ni:Va:W} = +0.52$ ${}^0T^C_{Ni:W:Va} = +633$ ${}^0B^{magn}_{Ni:W:Va} = +0.52$ ${}^0G_{Ni:W:Va} = +GHSERNI+0.125*GHSERWW-2100-1.56*T$ ${}^0G_{Ni:Va:W} = +GHSERNI+2.875*GHSERWW-2100$ ${}^0G_{Ni:W:W} = GHSERNI+GHSERWW$ ${}^0G_{Ni:W,Va:*} = +19\,000+14*T$ ${}^0G_{Ni:*:W,Va} = +19\,000+14*T$	This work [Eqs. (8–11)]
Ni_4W phase, model $(Ni)_4(W)$	$GHSERWW+4*GHSERNI-13600-4.15*T$	This work [Eq. (5)]
Ni_3W phase, model $(Ni)_3(W)$	$GHSERWW+3*GHSERNI-11000-2.17*T$	This work [Eq. (5)]

Table 5b. Thermodynamic parameters for the Ni–W system with interstitial Ni_8W.

Phase	Parameters (J(mol)$^{-1}$)	Source
Liquid phase, model (Ni,W)	${}^0L_{Ni,W} = -20\,470+7.55*T$ ${}^1L_{Ni,W} = -33\,545+15.2*T$ ${}^2L_{Ni,W} = -12\,400$	[54]
bcc_A2 phase, model $(Ni,W,Va)_1(Va)_3$	${}^0T^C_{Ni:Va} = 575$ ${}^0B^{magn}_{Ni:Va} = 0.85$ ${}^0L_{Ni,W} = +82\,000$	[55]
fcc_A1 phase, model (Ni,W)(Va)	${}^0T^C_{Ni:Va} = 633$ ${}^0B^{magn}_{Ni:Va} = 0.52$ ${}^0L_{Ni,W} = +2\,556+11.6*T$ ${}^1L_{Ni,W} = -52\,900$	[55]
Ni_8W phase, model $(Ni)_{0.889}(W,Va)_{0.111}$	${}^\circ T^C_{Ni:Va} = +633$ ${}^\circ B^{magn}_{Ni:Va} = 0.52$ ${}^\circ G_{Ni:W} = 0.889*GHSERNI+0.111*GFCCWW-24\,300+21*T$ ${}^0G_{Ni:W,Va} = 40\,000$ ${}^1G_{Ni:W,Va} = 90\,000$ ${}^2G_{Ni:W,Va} = 300\,000$	This work [Eqs.(11–12)]
Ni_4W phase, model $(Ni)_4(W)$	$GHSERWW+4*GHSERNI-91400+56.25*T$	This work [Eq. (5)]
Ni_3W phase, model $(Ni)_3(W)$	$GHSERWW+3*GHSERNI-69000+42.71*T$	This work [Eq. (5)]

Ni_4W and Ni_3W. Values for Ni_8W exhibit higher discrepancy, but the match between values is considered to be satisfactory. With interstitial Ni_8W, the Gibbs energies were about double to other cases. Table 4 summarises the analysed compounds in the Ni–W system and their structural data [7, 14, 15, 18, 21, 41, 61–63].

The assessed Ni–W phase diagram is shown in Fig. 5a with all these possible phases and in Fig. 5b without the Ni_8W phase (suppressed as metastable). Figure 5c was calculated with parameters using interstitially modeled fcc Ni_8W phase. Stability of phases was correct, except the solubility of tungsten in nickel was very small at low temperatures. Only calculations by Schindzielorz at al. [3] support that solubility can be very small especially below 500 K. However, this Ni–W system is a subsystem for the Ni–Ti–W system, where stable fcc-Ni and metastable fcc-Ni_3Ti phases exist. Ni_8W is thus a third fcc type phase [54, 64], and correcting the solubility of tungsten in fcc-Ni may cause a need to remodel fcc-Ni_3Ti. Therefore, the authors prefer martensitic Ni_8W modeling.

The superimposed diagrams are also shown in Fig. 6a and b where both fcc-A1 (Ni) solid solution and Ni_8W coexist or only fcc-A1 (Ni) solid solution is present. At elevated temperatures ($T > 1\,260$ K) the fit with experimental data is rather good (Fig. 6a). Figure 6b shows that the solubility of tungsten in nickel by Hofmann [29] was reported smaller than in these calculations. At 873 K the experimental point from Kornilov and Budberg [28] shows smaller solubility of tungsten in nickel than what is calculated here, and at 673 K the phase boundary matches very well to the Ni_8W phase boundary and quite well with fcc Ni solid solution boundary. Data by Gabriel et al. [30] agree well with the calculated eutectoid point at the Ni_8W–Ni_4W equilibrium line and also with Ni–W solid solution limits. Also calculated data by Kaufman and Nesor [65] agree well with the eutectoid temperature obtained by the present assessment. For tungsten solubility in nickel, Ellinger and Sykes [27] presented the same data point as in [65], where the latter shows too high solubility compared to the presently evaluated values. At 1 073 K Kornilov and Budberg [28] data (same as Hansen [66]) show too small solubility of tungsten in nickel. The fit between Meshkov et al. [34] experimental activity of tungsten data measured with galvanic cell and thermodynamic assessment is quite good. Table 5a (martensitic Ni_8W) and Table 5b (interstitial Ni_8W) show thermodynamic parameters for Ni–W system evaluated in this work. For the first time Ni_8W and Ni_3W were included in this Ni–W thermodynamic assessment. The phase diagram obtained from our assessment is consistent with first principles calculations and experimental data. Table 6a (martensitic Ni_8W) and Table 6b (interstitial Ni_8W) show the predicted reaction scheme for the Ni–W system: reactions, reactions type, calculated composition and temperature. The last column shows temperatures from independent literature data for comparison.

5. Conclusions

A set of consistent thermodynamic parameters for solution phases and intermetallic compounds was obtained for the Ni–W system by combining a literature review with our first principles calculations and thermodynamic assessment using the CALPHAD method from 298 K.

The best fit comparing calculated and experimental data for fcc-A1(Ni) solid solution boundary was achieved at elevated temperatures, with a very good correlation with the experimental phase diagrams from the literature, especially with the phase diagram containing Ni_8W as a (meta)stable phase, correlated with experimental data, where available. The fit between experimental and calculated tungsten activity in fcc nickel was quite good in the composition region 0–10 at.% tungsten.

The Ni_4W and Ni_3W phases were re-assessed thermodynamically as stoichiometric compounds in the present work. As NiW and NiW_2 phases were reported actually to be carbides Ni_6W_6C and Ni_2W_4C, respectively, they were not included in the binary Ni–W diagram.

It was found that the Ni_8W (prototype tetragonal Pt_8Ti) phase might have the same structure as $Fe_{16}C_2$ and $Fe_{16}N_2$,

Table 6a. Predicted reactions for the Ni–W system. Ni_8W modeled as martensitic phase. All reactions are at invariant points.

Reaction	Type	T (K)	Composition x (W)	Literature data T (K)
L → fcc-A1+bcc-A2	eutectic	1 768	0.208	1 766 [30, 33]
fcc-A1+bcc-A2 → Ni_4W	peritectoid	1 289	0.2	1 275 [42]
fcc-A1 → Ni_8W+Ni_4W	eutectoid	796	0.12	800 [3, this work]
Ni_4W+bcc-A2 → Ni_3W	peritectoid	848	0.25	850 [14, 15]

Table 6b. Predicted reactions for the Ni–W system. Ni_8W modeled as interstitial phase. All reactions are at invariant points.

Reaction	Type	T (K)	Composition x (W)	Literature data T (K)
L → fcc-A1+bcc-A2	eutectic	1 768	0.207	1 766 [30, 33]
fcc-A1+bcc-A2 → Ni_4W	peritectoid	1 289	0.2	1 275 [42]
fcc-A1 → Ni_8W+Ni_4W	peritectoid	804	0.11	800 [3, this work]
Ni_4W+bcc-A2 → Ni_3W	peritectoid	848	0.25	850 [14, 15]

which are both martensitic phases. This allowed us to assess these phases in a similar way with three sublattices and modified parameters and Gibbs energy functions for Ni : Va : W and Ni : W : Va sublattices. Two scenarios were used: one in which Ni_8W is stable and another in which Ni_8W was considered metastable and therefore not present in the equilibrium phase diagram. Both versions indicate that stable and metastable Ni_8W are in good agreement with independent experimental data. Ni_8W was also modeled as interstitial solid solution, but the solubility of tungsten in nickel was very small at low temperatures and there are no supporting experimental data. Also, calculated Gibbs energies of formation for compounds at 298 K are too high. Therefore, martensitic Ni_8W is preferred in this study.

Authors thank Dr. Reza Naraghi from Department of Materials Science and Engineering, KTH, Sweden for the help with the Fe–C TDB file.

References

[1] R.J. Mitchell, M. Preuss, S. Tin, M.C. Mardy: Mater. Sci. Eng. A – Struct. 473 (2008) 158 – 165. DOI:10.1016/j.msea.2007.04.098
[2] M.F. Ashby, D.R.H. Jones: Engineering Materials 1, An Introduction to Their Properties and Applications, Pergamon Press, Oxford (1989) 98 – 99.
[3] N. Schindzielorz, K. Nowak, S.B. Maisel, S. Müller: Acta Mater. 75 (2014) 307 – 315. DOI:10.1016/j.actamat.2014.04.029
[4] P.R. Mallory & Co., Inc. W-Ni-Fe-Mo Alloys. US Patent: us 3988118 (1976), 7 pp.
[5] L. Chen, P. Ettmayer, W. Lengauer: Z. Metallkd. 89 (1998) 83 – 89.
[6] P. Indyka, E. Beltowska-Lehman, L. Tarkowski, A. Bigos, E. Garcia-Lecina: J. Alloys Compd. 590 (2014) 75 – 79. DOI:10.1016/j.jallcom.2013.12.085
[7] R.H. Taylor, S. Curtarolo, G.L.W. Hart: J. Am. Chem. Soc. 132 (2010) 6851 – 6854. DOI:10.1021/ja101890k
[8] N. Tsyntsaru, H. Cesiulis, E. Pellicer, J.-P. Celsi, J. Sort: Electrochim. Acta 104 (2013) 94 – 103. DOI:10.1016/j.electacta.2013.04.022
[9] N. Sulitanu: J. Magn. Magn. Mat. 231 (2001) 85 – 93. DOI:10.1016/S0304 – 8853(01)00041 – 5
[10] G. Kresse, J. Furthmüller: Comp. Mater. Sci. 6 (1996) 15 – 50. DOI:10.1016/0927 – 0256(96)00008 – 0
[11] G. Kresse, J. Furthmüller: Phys. Rev. B 54 (1996) 11169 – 11186. DOI:10.1103/PhysRevB.54.11169
[12] J.P. Perdew, K. Burke, M. Ernzernhof: Phys. Rev. Lett. 77 (1996) 3865 – 3868. PMid:10062328; DOI:10.1103/PhysRevLett.77.3865
[13] D. Lerch, O. Wieckhorst, G.L.W. Hart, R.W. Forcade, S. Müller: Modelling Simul. Mater. Sci. Eng. 17 (2009), 19 pp. DOI:10.1088/0965-0393/17/5/055003
[14] S.J.B. Kurz, S.B. Maisel, A. Leineweber, M. Höfler, S. Müller, E.J. Mittemeijer: J. Appl. Phys. 116 (2014) 083515-1-083515-9. DOI:10.1063/1.4894148
[15] S.J.B. Kurz: Dr. Thesis, Nanocrystalline Thin Films: Microstructure, Stability and Properties, Max-Planck-Institut für Intelligente Systeme, Stuttgart, DEU (2014).
[16] Z.W. Lu, B.M. Klein: Phys. Rev. B 50 (1994) 5962 – 5970. DOI:10.1103/PhysRevB.50.5962
[17] G.B. Brook, Chapter 6, Crystal Chemistry, in: E.A. Brandes (Ed.), Smithells Metals Reference Book, 6th Edition, Butterworths, London (1983) 6-28-6-30.
[18] G.B. Brook, Chapter 6, Crystal Chemistry, in: E.A. Brandes, G.B. Brook (Eds.), Smithells Metals Reference Book, 7th Edition, Butterworth-Heinemann, Oxford (1999) 6-28-6-30.
[19] R. Naraghi, M. Selleby, J. Ågren: CALPHAD 46 (2014) 148 – 158. DOI:10.1016/j.calphad.2014.03.004
[20] G. Badinier: Ph. D. Thesis, University of British Columbia, Canada, (2013).
[21] F. Cardarelli, Materials Handbook, 2nd Ed., Springer, London (2008) 1219. DOI:10.1007/978-1-4471-3648-4
[22] S. Ishida, K. Kiwatase, S. Fujii, S. Asano: J. Phys.–Condens. Mat. 4 (1992) 765 – 774. DOI:10.1088/0953-8984/4/3/016765-774
[23] T. Kakeshita, C.M. Wayman: Mat. Sci. Eng. A 141 (1991) 209 – 219. DOI:10.1016/0921-5093(91)90771-E
[24] W. Kohn: Phys. Rev. 136 (1964) B864 – B871. DOI:10.1103/PhysRev.136.B864
[25] G. Kresse, D. Joubert: Phys. Rev. B 59 (1999) 1758 – 1775. DOI:10.1103/PhysRevB.59.1758
[26] K. Parlinski, Z.Q. Li, Y. Kawazoe: Phys. Rev. Lett. 78 (1997) 4063 – 4066. DOI:10.1103/PhysRevLett.78.4063
[27] F.H. Ellinger, W.P. Sykes: T. Am. Soc. Metal. 28 (1940) 619 – 645.
[28] I.I. Kornilov, P.D. Budberg: Dokl. Akad. Nauk SSSR 100 (1955) 73 – 75.
[29] H. Hofmann: Dissertation, Technische Universität Berlin, DEU (1983).
[30] A. Gabriel, H.L. Lukas, C.H. Allibert, I. Ansara: Z. Metallkd. 76 (1985) 589 – 595.
[31] W.B. Pearson: A Handbook of Lattice Spacings and Structures of Metals and Alloys, Vol. 4., Pergamon, Oxford UK (1958) 794.
[32] C. Laugee, C.H. Allibert, I. Ansara: Z. Metallkd. 76 (1985) 138 – 142.
[33] A.L. Udovskii, V.N. Karpushkin, E.A. Nikishina: Izv. Akad. Nauk. SSSR, Metall. (1991) 87 – 103.
[34] C.L. Meshkov, L.S. Guzei, V.A. Kasakov, M. Sokolovskaya: Mosc. Univ. Chem. Bull. 27 (1972) 83 – 84.
[35] J. Mayer, K. Urban: Phys. Status Solidi A 90 (1985) 469 – 475. DOI:10.1002/pssa.2210900209
[36] V. Subramanya Sarma, J. Eickemeyer, C. Mickel, L. Schultz, B. Holzapfel: Mat. Sci. Eng. A-Struct. 380 (2004) 30 – 33. DOI:10.1016/j.msea.2004.05.024
[37] S.B. Maisel, N. Schindzielorz, S. Müller, H. Reichert, A. Bosak: J. Appl. Cryst. 46 (2013) 1211 – 1215. DOI:10.1107/S0021889813016270
[38] R. Vogel: Z. Anorg. Chem. 116 (1921) 231 – 242. DOI:10.1002/zaac.19211160123
[39] K. Becker, F. Ebert: Z. Phys. 16 (1923) 165 – 169. DOI:10.1007/BF01327387
[40] R. Cury, J.-M. Joubert, S. Tusseau-Nenez, E. Leroy, A. Allavena-Valette: Intermetallics 17 (2009) 174 – 178. DOI:10.1016/j.intermet.2008.11.001
[41] S. Inomata, M. Kajihara: J. Alloys Compd. 509 (2011) 4958 – 4966. DOI:10.1016/j.jallcom.2011.01.139
[42] H. Okamoto: Desk Handbook, Phase Diagrams for Binary Alloys, ASM International, Materials Park, Ohio, USA (2000) 626.
[43] L.P. Arapova: Sov. Phys. J. 16 (1973) 1173 – 1175. DOI:10.1007/BF00890486
[44] H. Okamoto: Desk Handbook, Phase Diagrams for Binary Alloys, ASM International, Materials Park, Ohio, USA (2000) 572. PMid:11198271
[45] Ya.S. Umanskii, A.N. Dubrovina, L.P. Arapova: Izv. VUZov, Chern. Metall. 11 (1969) 129 – 131 (cited by Hofmann [29]).
[46] L.P. Arapova: Sov. Phys. J. 19 (1976) 1197 – 1199. DOI:10.1007/BF00891478
[47] J.M. Walsh, M.J. Donachie: Metall. Trans. 4 (1973) 2854 – 2855. DOI:10.1007/BF02644589
[48] X. Liu, J. Pilling, R.W. Heckel, J.K. Lee: Mat. Sci. Tech. Ser. 7 (1991) 228 – 237. DOI:10.1179/mst.1991.7.3.228
[49] J. Lee, C.R. Lear, Z. Zhang, P. Bellon, R.S. Averback: Metall. Mater. Trans. A 46A (2015) 1046 – 1061. DOI:10.1007/s11661-014-2704-4
[50] C.J. Marvel, P.R. Cantwell, M.P. Harmer: Scripta Mater. 96 (2015) 45 – 48. DOI:10.1016/j.scriptamat.2014.10.002
[51] K.E. Poulsen, S. Rubæk, E.W. Langer: Scripta Metall. Mater. 8 (1974) 1297 – 1300. DOI:10.1016/0036-9748(74)90349-4
[52] P.E. Blöchl: Phys. Rev. B 50 (1994) 17953 – 17979. DOI:10.1103/PhysRevB.50.17953

[53] J.P. Perdew, K. Burke, M. Ernzernhof: Phys. Rev. Lett. 78 (1997) 1396–1396. DOI:10.1103/PhysRevLett.78.1396
[54] N. Dupin: Personal communication, Ni-Ti-W TDB file, (2013).
[55] P. Gustafson, A. Gabriel, I. Ansara: Z. Metallkd. 78 (1986) 151–156.
[56] A.T. Dinsdale: CALPHAD 15 (1991) 317–425. DOI:10.1016/0364-5916(91)90030-N
[57] O. Redlich, A.T. Kister: Ind. Eng. Chem. 40 (1948) 345–348. DOI:10.1021/ie50458a036
[58] J.O. Andersson, T. Helander, L. Höglund L., P.F. Shi, B. Sundman: Calphad 26 (2002) 273–312. DOI:10.1016/S0364-5916(02)00037-8
[59] S. Jonsson: Ph.D. Thesis, Royal Institute of Technology, Stockholm, Sweden (1993).
[60] Y. Peng, P. Zhou, Y. Du, K. Chang: Int. J. Refract. Met. H. 40 (2013) 36–42. DOI:10.1016/j.ijrmhm.2013.03.012
[61] H. Okamoto: Desk Handbook, Phase Diagrams for Binary Alloys, ASM International, Materials Park, Ohio, USA (2000) 238.
[62] E. Parthe, L. Gelato, B. Chabot, M. Penzo, K. Cenzual, R. Gladyshevskii, TYPIX Standardised Data and Crystal Chemistry Characterization of Inorganic Structure Types, 4.3. Strukturbericht Table in: E. Fluck (ed.) Gmelin Handbook of Inorganic and Organometallic Chemistry, Springer Verlag, 8th Ed., Berlin, Heidelberg DEU (1993) 363–371.
[63] T. Hahn, in: D. W. Penfold, M. H. Dacombe, S. E. Barnes and N. J. Ashcroft (eds.) International Tables for Crystallography, Vol. A, Fifth Edition, The International Union for Crystallography by Springer, DEU (2005) 292, 356, 478, 688, 734.
[64] M.H. de Sa, I. Isomäki, J.A. Ferreira, M. Hämäläinen, M.H. Braga: Mater. Sci. Forum 730–732 (2013) 775–780.
[65] L. Kaufman, H. Nesor: Can. Metall. Quart. 14 (1975) 221–232. DOI:10.1179/000844375795050157
[66] M. Hansen, Constitution of Binary Alloys, 2nd Edition, McGraw-Hill, New York, (1958) 1058.

(Received October 28, 2016; accepted July 10, 2017; online since October 2, 2017)

Correspondence address

Iikka Isomäki Ph.D.
Department of Chemical and Metallurgical Engineering
School of Chemical Engineering
P.O. Box 16200
00076 Aalto University
Espoo
Finland
Tel.: +358 50 3772069
Fax: +358 9-47022659
E-mail: iikka.isomaki@aalto.fi
Web: http://materials.aalto.fi/en/

Bibliography
DOI 10.3139/146.111557
Int. J. Mater. Res. (formerly Z. Metallkd.)
108 (2017) 12; page 1025–1035
© Carl Hanser Verlag GmbH & Co. KG
ISSN 1862-5282